ISSN 0304-9892 (Print) ISSN 2455-7463 (Online)
www.vijnanaparishadofindia.org/jnanabha
***Jñānābha*, Vol. 52(2) (2022), 111-119**
(Dedicated to Professor D. S. Hooda on His 80th Birth Anniversary Celebrations)

SYNERGETIC EFFECT OF Sn^{3+} ON STRUCTURAL, OPTICAL AND DIELECTRIC PROPERTIES OF ZnO NANOSTRUCTURES

Anil Kaushik
Department of Physics, G.C.W. Gohana, Sonepat-131301, Haryana, India
Email: gphysics07@gmail.com

(Received: April 29, 2022*; In format: May* 06, 2022*; Accepted: October* 10, 2022*)*

DOI: https://doi.org/10.58250/jnanabha.2022.52213

Abstract

This work shows the impact of Sn^{3+} ion doping on structural, optical and dielectric properties of ZnO synthesized via co-precipitation technique. The synthesized samples were examined using *XRD* (X-ray Diffractometer), *FeSEM* (Field Emission Scanning Electron Microscope), *FTIR* (Fourier Transform Infrared Spectroscopy), *PL* (Photoluminescence) and Impedance Spectroscopy. The *XRD* patterns confirmed the hexagonal structure with P63mc space group and the crystalline sizes, strain and volume of cell are 37.4 nm, 2.5968Å and 59.85Å^3. The morphological micrographs were recorded via SEM. The photoluminescence spectra were measured using a photoluminescence spectrometer with a 325 nm excitation wavelength. *FTIR* (Fourier Transform Infrared Spectrometer) spectrometer was used to measure *IR* spectra in the range 500 – 3600 cm^{-1}. Complex impedance spectroscopy of the $Sn^{3+}/ZnO-400$ samples was performed at 310 K using a galvenostat in the frequency range of $5MHz$ to 50 Hz at applied voltage of $50mV$. The grain edge resistance of the $Sn^{3+}/ZnO-400$ sample is $14.57M\Omega$ (at 310 K).

2020 Mathematical Sciences Classification: 00A79, 78-05, 78A45.
Keywords and Phrases: Sn^{3+}, Zinc Oxide, *SEM*, Photoluminescence, *FTIR*, Complex Impedance.

1. Introduction

There is growing interest in combining carrier spin with charge to create a new class of devices such as spin light-emitting diodes, spin field effect transistors, spin qubits for quantum computers and spin-based memory systems [8]. Zinc oxide (ZnO), an II-VI oxide semiconductor with a direct and wide band gap (3.3 eV), has a high exaction binding energy (almost $60meV$ at ambient temperature), good transparency and long-term stability. Because of its excellent optoelectronic, sensing and piezoelectric capabilities, it has been given serious consideration. These appealing properties makes it a detecting metal oxide for a variety of applications such as gas sensors, solar energy storage, varistors, spintronic devices, photovoltaic, photocatalysts and light emitting diodes (LEDs) [8,9]. It is also one of the most biocompatible, biodegradable and bio-safe materials for medicinal and environmental applications. Since particle size and crystal morphology play such a big role in these applications, a lot of people are interested in how to make ZnO nanostructures. Nonetheless, doping with various impurity atoms is an effective technique to change the physical properties of the chemical under investigation [1,2]. The magnetic characteristics of Fe doped ZnO nanoparticles have attracted attention due to their ferromagnetic behavior at ambient temperature and possible application in spintronics [1, 2, 4]. Nonetheless, compared to its other features, the electrical properties of Sn doped ZnO nanoparticles have received less attention. Several studies have revealed changes in electrical and dielectric characteristics caused by the introduction of different dopant ions into the ZnO lattice in this context. Despite the fact that many studies on doped zinc oxide nanostructures exist, the influence of Sn doping on the electrical characteristics of ZnO nanoparticles has yet to be accounted for to our knowledge. We examined the effect of Sn doping on the structural, optical and electrical properties of ZnO nanoparticles.

2. Experimental Details

The samples in this investigation were made with $Zn(CH_3COO_2, SnO_2, NaOH, C_2H_5OH$, and DI water as early components. In the traditional co-precipitation production of Sn modified ZnO nanoparticles (abridged $Sn^{3+}/ZnO-RT \& Sn^{3+}/ZnO-400$), the preparatory ingredients or precursors were contracted in stoichiometric share of $Zn(CH_3COO)_2, SnO_2$ and $NaOH$. The precursors were dissolved in a solution of C_2H_5OH and DI water. The mixture of these preliminary components is stirred at 80°C for 2 hours. After that, the solution was allowed to lie overnight before being washed several times with distilled water and dried in a vacuum oven at 90°C for 12 hours. As a consequence, the powder was annealed for 2 hours at 400°C. The phase and crystal structure of manufactured $Sn^{3+}/ZnO-RT$ and $Sn^{3+}/ZnO-400$ samples were examined using Rigaku's X-ray Diffractometer (with $Cu-K\alpha$ as

a radiation source; $\lambda = 1.542$Å). With a scanning speed of 2% min, the scanning diffraction angle ranged from 10° to 90°. Surface morphology of $Sn^{3+}/ZnO - RT$ and $Sn^{3+}/ZnO - 400$ samples were investigated using SEM scans at a $20kV$ accelerating voltage. The energy band gap and emission spectra were determined using a photoluminescence (PL) spectrometer. The stretching bonds in the materials were discovered using FTIR spectroscopy. AC impedance was investigated using Galvanostat (Bio Logic; $SP240$).

3. Results and discussions

3.1. Structural analysis of Sn doped ZnO

Figure 3.1 shows the XRD spectrum for Sn^{3+} tailored ZnO structures in the 2θ range between 10° and 90° and the whole XRD data was matched and verified using the JCPDS file #80-0075, which shows the identical crystal planes as the hexagonal wurtzite structure of Zinc Oxide [12]. Figure 3.1 shows the XRD results of synthesized $Sn^{3+}/ZnO-RT$ and Sn^{3+}/ZnO sintered at $400°C$ samples of Sn^{3+} modified ZnO with diffraction angles ranging from 10 to 90 degrees and equivalent to hkl planes (100), (002), (101), (102), (103), (200), (112), (201) and (202). For the Sn^{3+} tailored ZnO, the Sn^{3+} modifies the diffraction peak by 0.02° in that order [12].

$$D(nm) = \frac{K * \lambda}{\beta_{1/2} * \cos\theta} \tag{3.1}$$

$$4d^2 \sin^2\theta = n^2\lambda^2 \tag{3.2}$$

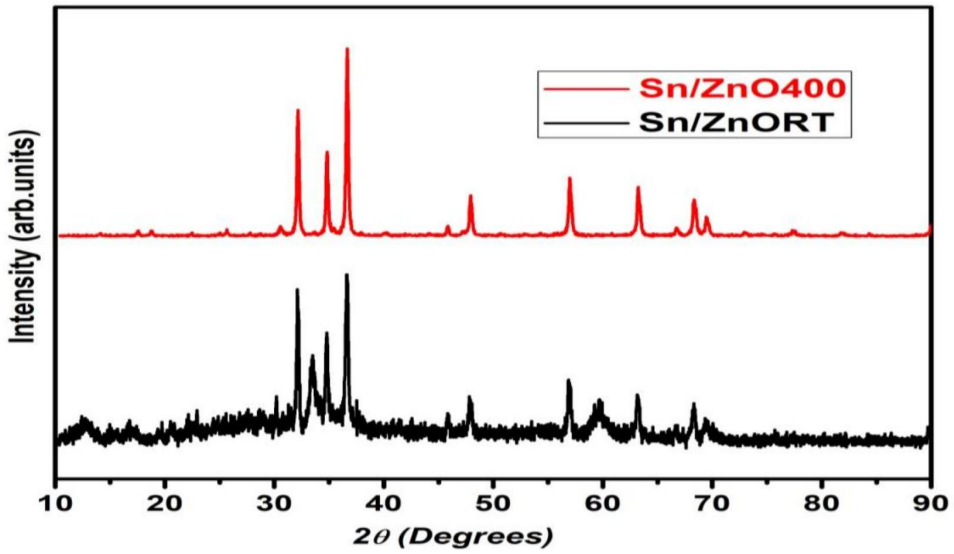

***Figure* 3.1:** XRD patterns of $Zn_{0.92}Sn_{0.08}O$ at room temperature $\left(Sn^{3+}/ZnO - RT\right)$ and calcined at $400°C\left(Sn^{3+}/ZnO - 400\right)$

where '$K = 0.89$', 'λ' is wavelength of X-ray, $\beta_{1/2}$ is the $FWHM$ and ' θ ' is Bragg angle. The phases of the ZnO lattice structure are primarily depicted by the significantly lower intensities of the XRD crest due to the oxides, as opposed to the bristly and climax with acute passion for the hexagonal structures. The extra particle values for Zinc based Oxide made from a range of prepared material dissolved in water are in admirable disagreement with the connote domain sizes for ZnO. Sn^{3+} substituted $ZnO-400$ particles have smaller domain sizes than unmodified ZnO, which is important for higher doping altitude. The $Sn - O - Zn$ bond on the domain surfaces of the Sn^{3+} modified Zinc based oxide crystals may be to blame for the mild increase in domain diameters, preventing crystal growth [6]. Furthermore, due to the discrepancy between the ionic radii of $Sn^{3+}(0.140\ nm)$ and $Zn(0.071\ nm)$ ions, the crystalline size decreases with Sn substitution, as reported by many others [6]. The inclusion of the Sn substituent in the lattices caused a change in the lattice variables as measured from the XRD data, as shown in Table 3.1.

***Table* 3.1:** Sn^{3+} doped zinc oxide with annealing and its lattice parameters

Sample	***Crystallite size (nm)***	***Inter planar spacing (d) Å***	***Lattice constant Å***		***Volume (V) Å³***	***X Ray Density (d_x) g/cm³***	***Lattice Strain η***
			a=b	**c**			
Sn/ZnO-RT	48.3	2.6743	3.7629	5.6453	70.34	8.06	0.0032
Sn/ZnO-400	37.4	2.5968	3.5578	5.3735	59.85	7.56	0.0053

3.2. Scanning electron microscopy of Sn doped ZnO nanostructures

The role of Sn^{3+} on the morphologies of $Sn^{3+}/ZnO-RT$ and $Sn^{3+}/ZnO-400$ is shown in Figure 3.2 (a-b), which was clicked out using SEM. The micrographs shown in the figure have a crystallite temperament and show agglomeration, asymmetric forms and sizes due to the significant chemical reaction with heat. Nanoparticles exhibit structural, electrical and other features thanks to their uneven particle shape. This appearance of upshot should be attributable to their lower diffusivity. These conclusions are further supported by the *XRD* analysis [6].

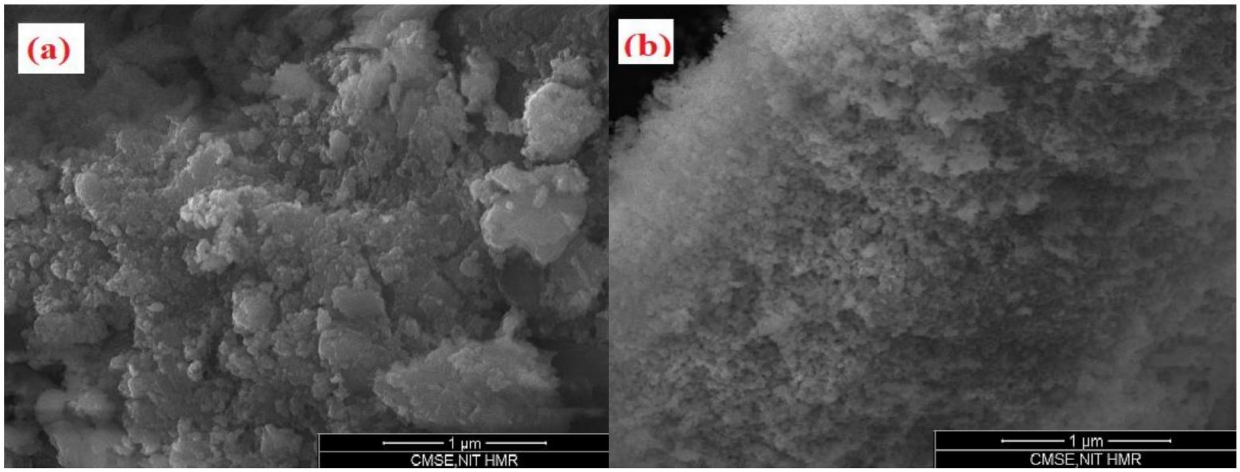

***Figure* 3.2:** SEM micrographs of (a) $Sn^{3+}/ZnO-RT$ (b) $Sn^{3+}/ZnO-400$ samples

3.3. Photoluminescence spectroscopy of Sn/ZnO

The photoluminescence (PL) spectra of $Sn^{3+}/ZnO-RT$ and $Sn^{3+}/ZnO-400$ samples with a deliberate excitation wavelength of 325 *nm* are shown in Figure 3.3.

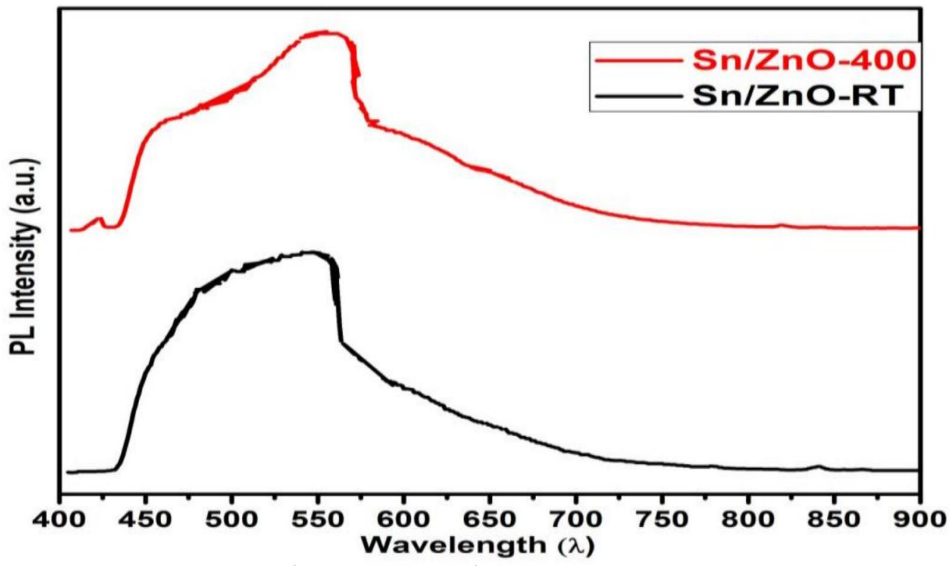

***Figure* 3.3:** *PL* spectrum of $Sn^{3+}/ZnO-RT$ and $Sn^{3+}/ZnO-400$ samples

There was strong emission crest centralization at about 420 *nm* and 550 *nm*, with red shifts correlated to Zinc Oxide's close-band emissions. This is due to defects in doped *ZnO* caused by the substitution of Sn^{3+} ions, which may result in the erecting of a small energy level near the conduction bands. The violet emission peaks might thus be sustained by the insignificant energy levels emitted at the recombination centers [8]. As a result of the change of Sn^{3+}, interstitial *Zn* ions and O_2 vacancies were formed differently, which had a significant impact on the optical character of the doping ion doped *ZnO* samples. At 425 *nm*, three different emissions are possible for undoped *ZnO*. Violet luminescence (434 *nm*) is attributed to the electronic transition from the interstitial *Zn* level (Zni) to the valence bands [10], because its peak energy ($2.85eV$) coincides with the planned band gap between the interstitial Zn level and the valence band peak (2.91 eV) [7] and the blue emission peak of 455 *nm*.

3.4. FTIR of Sn^{3+} doped $ZnO(Sn/ZnO-RT$ and $Sn/ZnO-400)$

In the 500-3600 cm^{-1} wave number region, Figure 3.4 displays the FTIR spectrum of $Sn^{3+}/ZnO-RTs$ & $Sn^{3+}/ZnO-400$ sample. 3350 cm^{-1}, 2350 cm^{-1}, 1530 cm^{-1}, 1425 cm^{-1}, 1203 cm^{-1}, 836 cm^{-1}, 610 cm^{-1}, and 539 cm^{-1} are the *IR* apex of the $Sn^{3+}/ZnO-RTs$ and $Sn^{3+}/ZnO-400$ materials, respectively.

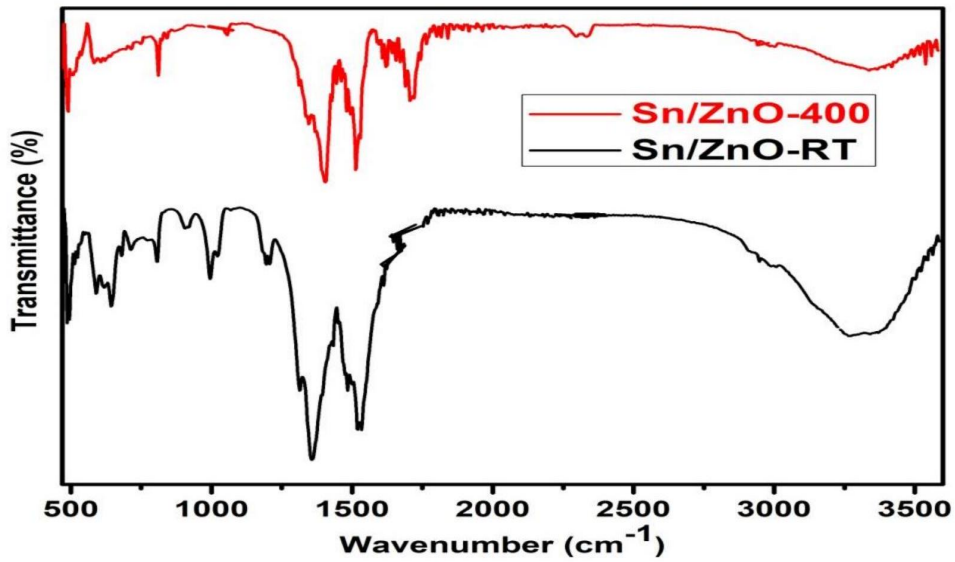

***Figure* 3.4:** FTIR Spectrum of $Sn^{3+}/ZnO - RT$ and $Sn^{3+}/ZnO - 400$ samples

The vibrations of the $C - H, C = O$ and $C - O$ bonds are represented by the IR dip in the 682 cm^{-1} to 1645 cm^{-1} range. The tiny and scruffy absorptions band at 830 cm^{-1} account for the rare state next to Sn^{3+} in the $Zn - O$ lattice structure. The elongation of the $Zn - O$ bonds is seen in the peaks between 539-650 cm^{-1} [7]. The remaining peaks, which span from 1700 cm^{-1} to 3295 cm^{-1} and indicate $O - H$ bond stretching vibrations, submerged water bending modes and $O = C = O$ bond availabilities, are in the 1700 cm^{-1} to 3295 cm^{-1} range. The presence of quenchable stress on Sn^{3+}/ZnO nanocrystallines, increase in Sn^{3+}/ZnO crystallite character and differentiation in Sn^{3+}/ZnO morphologies, as evidenced by the Sn^{3+}/ZnO sample XRD pattern and SEM images. This causes the FTIR crest to appear piercingly in the variation of wave number from 500 cm^{-1} to 1500 cm^{-1} as the calcination temperature rises for the Sn/ZnO.

3.5. Complex Impedance Spectroscopy

The complex impedance experiment is a well-known method of determining the electrical conductance character of a sample in relation to its structures, as well as the spectrum of electronic states. Figure 5 (a) shows the complex impedance $(Z + iZ\ )$ graphs of the $Zn_{0.92}Sn_{0.08}O\left(Sn^{3+}/ZnO - 400\right)$ sample in the 50 Hz to $05MHz$ frequency range with the field $50mV$ applied at 310 K

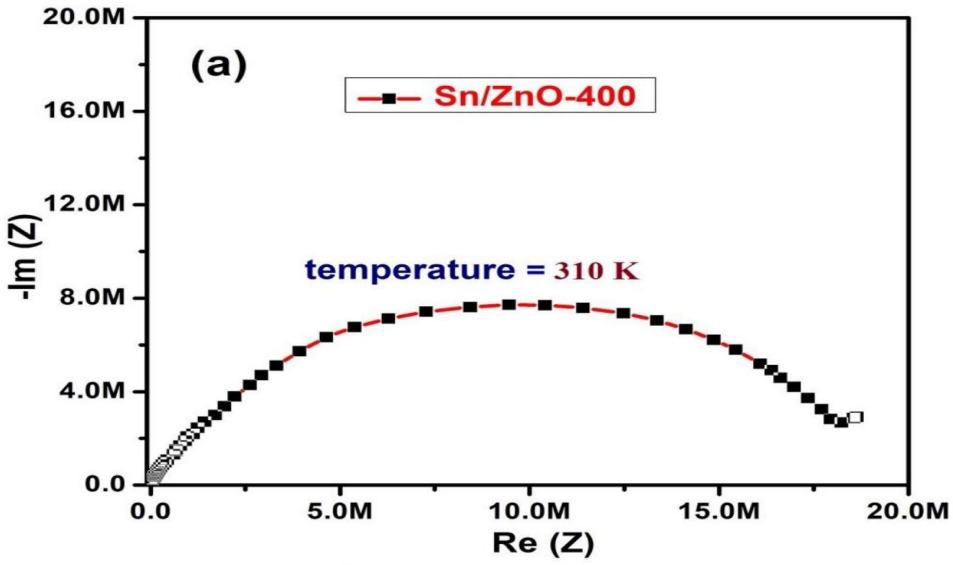

***Figure* 3.5:** (a) Nyquist plot of Sn^{3+}/ZnO – 400 sample at room temperature (310 K).

In order to avoid electric transport ambitious by visible light in the Sn^{3+}/ZnO – 400 samples, the impedance spectrum is mapped in the absence of light. Normally, the grain corollary produces a second semicircle curve that is appended to the complex impedance curve [11]. Thermally activated charge carriers have enough energy to exceed the isolating domains' limit and devote electrical conduction in this type of semiconducting material activity. There are two forms of dielectric relaxation phenomena or non-Debye form behavior in semicircles, according to Nyquist graphs [3]. Figure 3.5(b) depicts the variance of the real fraction (Z') of the complex AC impedance as a frequency function at 310 K. It is clear from the figures that as the frequency function increases, the values of Z ' abruptly decrease, indicating increased AC conductivities due to hopping conduction phenomena [11]. The real component of complex impedance has a contingent efficiency of hard frequencies in the lower frequency province, which correlates to high resistivity values and greater grain boundary resistance values, while Z ' operates at sovereign frequencies in the upper frequency range. Figure 3.5 (c) shows the variation of impedance imz fraction (Z'') as a function of frequency, illustrating that the behavior is the same as Z'. Complex AC Impedance Spectroscopy is used to align the low and high frequency dispersal zones to shred the domain or grain and domains periphery of the crystal structures [3, 11]. The Nyquist (cole-cole) graph shows a single semicircular curvature, indicating the presence of domains or grains in manufactured ZnO samples and a separate relaxation mechanism. The arc interacts with the domain boundaries at lower frequencies, whereas the grain is governed by the arc at higher frequencies. It demonstrates how domain, grain and electrode interface resistance reduces. When the temperature rises, the relaxation time decreases and the conductivity increases.

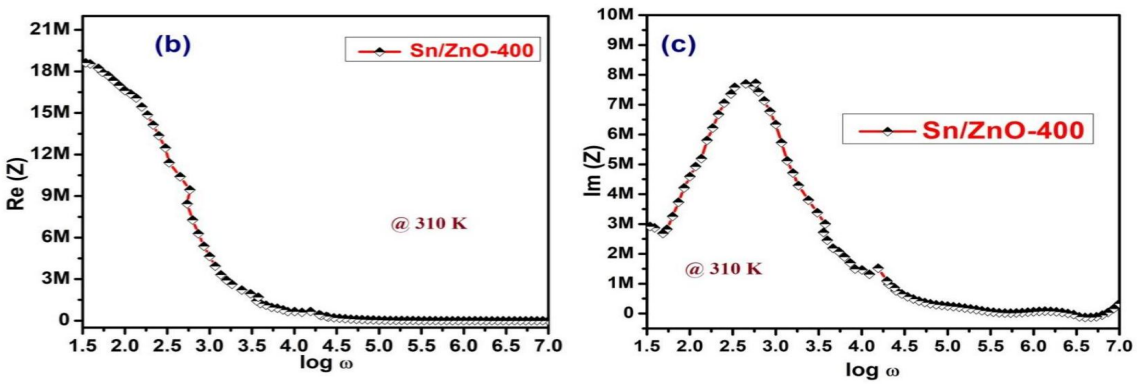

***Figure* 3.6:** Variation of (b) Real part (Z') (c) Imz part (Z') of impedance v/s frequency ($\log \omega$) at room temperature.

3.6. Dielectric studies

The dielectric constant varies with frequency, as shown in figure 3.6. According to the literature, the dielectric constant grows continuously as the temperature rises in the inferior frequency areas, implying a significant dielectric dispersion generated by thermally promoted charges like space charges, charged deficiencies and charged charges.

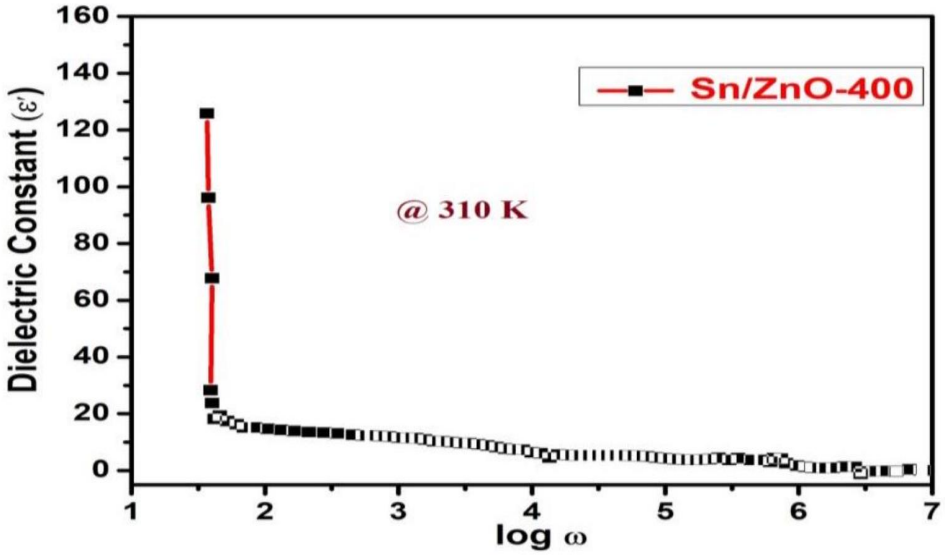

***Figure* 3.7:** Variation of Dielectric Constant v/s frequency ($\log \omega$) at room temperature for $Sn^{3+}/ZnO - 400$ sample.

The dielectric constant increases as the amount of Sn increases, displaying monotonous rising characteristics with increasing frequencies at the same temperature. Defect-related dipoles can be followed by alternating current at low frequencies, resulting in high dielectric constants (strong dielectric dispersions region). As the frequencies increase, the dielectric constant begins to lag behind the applied field, reducing the dielectric constants (plateau regions) and reaching nearly constant values. This action was sculpted by Koop's phenomenological theory and Maxwell-space Wagner's charge polarizations [3]. Dipoles freeze at low temperatures due to a space charge relaxation mechanism at the interfaces that causes reduced polarizations, resulting in a small dielectric constant value [7]. The accessible free charges provided in the application of the area in question observe the polarization of space charges. As a result, as frequency decreases, the dielectric constant increases. Furthermore, the larger sample dielectric constants are attributable to oxygen vacancies created by Sn^{3+} substitution during charge compensations [3, 11]

3.7. AC conductivity analysis

The AC electrical conductivities of $Sn^{3+}/ZnO-400$ nanostructures as a function of frequencies are examined at 310 K in order to determine the conductions mechanism and charge carrier type responsible for this activity. The following equation describes the AC conductivities of $Sn^{3+}/ZnO - 400$(3)[5]

$$\sigma_{ac}(\omega) = \omega \varepsilon_o \varepsilon' \tan\delta \tag{3.3}$$

where ω is the angular frequency, ε_o is the permittivity of free space and $\tan\delta$ is the relaxation loss. The frequency spectrum ($5MHz - 50\ Hz$) was used to investigate the relationship between relaxations and conductivity efficiency, as well as the effect of Sn replacement in ZnO samples. The frequency-dependent graphs of AC conductivity with frequency variance are shown in Figure 3.7. Conductivity has been found to increase with frequency. In the lower frequencies area (plateau areas), the plot $\log(\sigma_{AC})\ v/s \log(\omega)$ indicates that the plots are frequencies sovereign (Approx. Flat plot), demonstrating the influence of DC conductions in $Sn^{3+}/ZnO - 400$. Because of charge carrier hopping, which is studied by Koop's phenomenological assumption, AC conductivities increase as the frequency of the applied field increases [3, 5]. AC conductivities rise with temperature because charge defects such as O_2 vacancy ionisation and thermally induced charge carriers cause high temperature conductions and relaxations [5]. When ZnO is doped with Sn^{3+}, its conductivity falls, as illustrated in Figure 3.7. The oxygen vacancy in the sample increases as substitution concentrations rise, producing in larger free electron densities and AC conductivities [3]. To monitor interfacial polarizations, free electrons are usually captivated inside the domain boundaries of ferroelectric

materials. During ferroelectric transitions, the absorbed electrons would be released, which could explain the rise in conductivity [5, 11]. Figure 3.7 depicts the difference in frequency-dependent AC conductivities of the $Sn^{3+}/ZnO{-}400$ nanostructures at ambient temperatures. That is to say, as the frequency increases, the conductivity of all materials is seen to increase. As the frequencies of the applied fields increase, so does the hopping of charge carriers, resulting in higher conductivities. The increase in AC frequencies conductivity is due to interfacial polarizations, as anticipated by Koop's phenomenological conjecture [5], implying that Sn^{3+}/ZnO samples function as a multilayer capacitor. Conductivities are caused by domain boundaries at low frequencies, while dispersions are caused by conducting domains at higher frequencies. At 310 K, the conductivity ($\log \sigma(\omega)$) for $Sn^{3+}/ZnO - 400$ is $-7.3(\Omega - cm)^{-1}$.

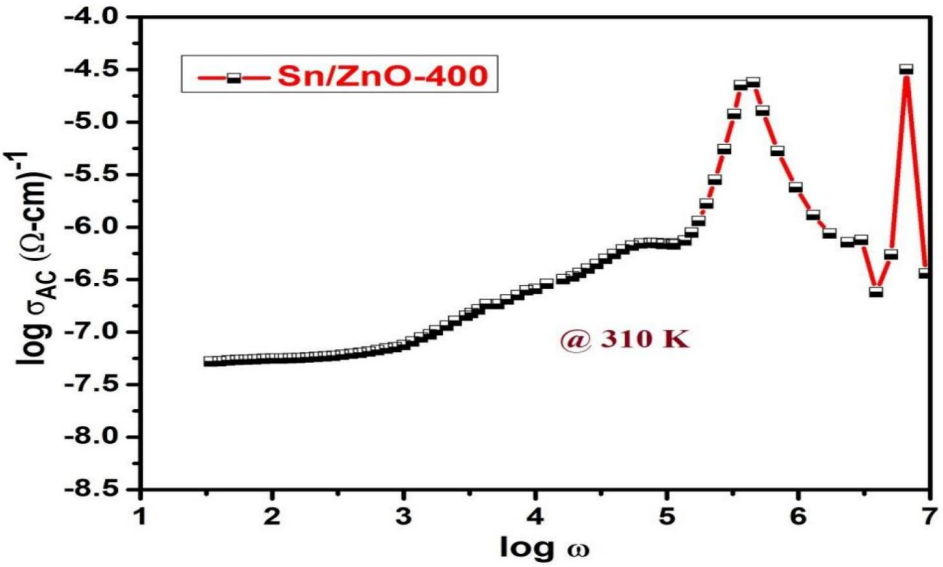

***Figure* 3.8:** Variation of AC conductivity v/s frequency ($\log \omega$) at room temperature for $Sn^{3+}/ZnO - 400$ sample

4. Conclusion

To investigate the effect of temperature on material preparation and properties, Sn doped ZnO samples were profitably synthesized using the co-precipitation technique at various sintering temperatures. XRD (X-Ray Diffractions) data confirm the hexagonal structure of wurtzite with space group $P63mc$. The Sn doped ZnO at $400°C$ sample's domain size, intra-plane spacing and cell volume were determined to be 37.4 nm, 2.5968 nm and 59.85Å^3 respectively. Surface morphology studies were all carried out using FESEM (Field emission scanning electron microscope). A photoluminescence spectrometer with a 325 nm excitation wavelength was used to measure the photoluminescence spectra. As a result of the stretching of the $Zn - O$ bonds, FTIR spectrometer was utilized to analyze IR spectra with peaks. The vibrations of the C - H, $C = O$ and $C - O$ bonds are represented by the IR dip in the range 682 cm^{-1} to 1645 cm^{-1}. At 310 K, Sn doped ZnO at $400°C$ samples were subjected to complex impedance spectroscopy employing a galvenostat/potentiostat in the $5MHz$ to 50 Hz frequency range. Grain margin resistance for Sn doped ZnO at $400°C$ is $14.57M\Omega$ and the conductivity ($\log \sigma(\omega)$) is $-7.3(\Omega\ cm)^{-1}$ (at room temperature, 310 K). The findings motivated the researcher to look into rare earth metal doped ZnO nanostructures for a number of applications.

Acknowledgement. Author is grateful to the Department of Physics, Baba Mastnath University, Rohtak, India for providing the necessary facilities.

References

[1] A. K. Arora, S. Devi, V. S. Jaswal, J. Singh, M. Kinger and V. D. Gupta, Synthesis and characterization of ZnO nanoparticles, *Oriental Journal of Chemistry,* **30**(4) (2014), 16711679.

[2] R. Chauhan, A. Kumar, R. P. Chaudhary and T. Education, Synthesis and characterization of silver doped ZnO nanoparticles, *Archives of Applied Science Research,* **2**(5) (2010), 378-385.

[3] M. L. Dinesha, G. D. Prasanna, C. S. Naveen, H. S. Jayanna, Structural and dielectric properties of Fe doped ZnO nanoparticles, *Indian Journal of Physics,* **87**(2) (2013), 147153.

[4] Li-Hua Li, Jian-Cheng Deng, Hui-Ren Deng, Zi-Ling Liu and Ling Xin, Synthesis and characterization of chitosan/ZnO nanoparticle composite membranes, *Carbohydrate Research,* **345**(8) (2010), 994-998.

[5] M. M. Hassan, W. Khan, A. Azam and A. H. Naqvi, Influence of Cr incorporation on structural, dielectric and optical properties of *ZnO* nanoparticles, *Journal of Industrial and Engineering Chemistry,* **21** (2015), 283-291.

[6] W. Khan, Z. A. Khan, A. A. Saad, S. Shervani, A. Saleem and A. H. Naqvi, Synthesis and characterization of Al doped *ZnO* nanoparticles, *International Journal of Modern Physics Conference Series,* **22** (2013), 630-636, World Scientific Publishing Company.

[7] A. S. Lanje, S. J. Sharma, R. S. Ningthoujam, J. S. Ahn and R. B. Pode,, Low temperature dielectric studies of zinc oxide (*ZnO*) nanoparticles prepared by precipitation method, *Advanced Powder Technology,* **24**(1) (2013), 331-335.

[8] S. B. Rana, P. Singh, A. K. Sharma, A. W. Carbonari and R. Dogra, Synthesis and characterization of pure and doped ZnO nanoparticles, *Journal of Optoelectronics and Advanced Materials,* **12**(2) (2010), 257-261.

[9] R. Song, Y. Liu and L. He, Synthesis and characterization of mercaptoacetic acid-modified ZnO nanoparticles, *Solid State Sciences,* **10**(11) (2008), 1563-1567.

[10] T. Sahoo, M. Kim, J. H. Baek, S. R. Jeon, J. S. Kim, Y. T. Yu and I. H. Lee, Synthesis and characterization of porous *ZnO* nanoparticles by hydrothermal treatment of as pure aqueous precursor, *Materials Research Bulletin,* **46**(4) (2011), 525-530.

[11] D. Varshney, K. Verma and S. Dwivedi, Structural and dielectric studies of hexagonal *ZnO* nanoparticles, *Optik,* **126**(23) (2015), 4232-4236.

[12] D. W. Zeng, C. S. Xie, B. L. Zhu, W. L. Song and A. H. Wang, Synthesis and characteristics of Sb-doped *ZnO* nanoparticles, *Materials Science and Engineering*: *B*, **104**$(1-2)(2003), 68-72$.